REPORT DOCUMENTATION PAGE

Form Approved OMB NO. 0704-0188

1. REPORT DATE (DD-MM-YYYY)	2. REPORT TYPE	3. DATES COVERED (From - To)
	New Reprint	-

4. TITLE AND SUBTITLE
A COMPLEX NETWORK ANALYSIS OF GRANULAR FABRIC EVOLUTION IN THREE-DIMENSIONS

5a. CONTRACT NUMBER
W911NF-07-1-0370

5b. GRANT NUMBER

5c. PROGRAM ELEMENT NUMBER
611102

6. AUTHORS
Sebastian Pucilowski, David M. Walker, Antoinette Tordesillas

5d. PROJECT NUMBER

5e. TASK NUMBER

5f. WORK UNIT NUMBER

7. PERFORMING ORGANIZATION NAMES AND ADDRESSES
University of Melbourne
Melbourne Research
Swanston Street

8. PERFORMING ORGANIZATION REPORT NUMBER

9. SPONSORING/MONITORING AGENCY NAME(S) AND ADDRESS(ES)
U.S. Army Research Office
P.O. Box 12211
Research Triangle Park, NC 27709-2211

10. SPONSOR/MONITOR'S ACRONYM(S)
ARO

11. SPONSOR/MONITOR'S REPORT NUMBER(S)
51924-EV.18

12. DISTRIBUTION AVAILIBILITY STATEMENT
Approved for public release; distribution is unlimited.

13. SUPPLEMENTARY NOTES
The views, opinions and/or findings contained in this report are those of the author(s) and should not contrued as an official Department of the Army position, policy or decision, unless so designated by other documentation.

14. ABSTRACT
Recent studies employing graph theoretic techniques from Complex Networks revealed the co-evolution of emergent minimal contact cycles
and load-bearing force chains as mesoscopic structures that form the basic
building blocks of self-organization. This study demonstrates previously observed trends for two-dimensional assemblages of circular discs to equally

15. SUBJECT TERMS
Granular media, complex networks, particles, stability, discreteelement method

16. SECURITY CLASSIFICATION OF:			17. LIMITATION OF ABSTRACT	15. NUMBER OF PAGES	19a. NAME OF RESPONSIBLE PERSON
a. REPORT	b. ABSTRACT	c. THIS PAGE			Antoinette Tordesillas
UU	UU	UU	UU		19b. TELEPHONE NUMBER 038-344-9685

Report Title

A COMPLEX NETWORK ANALYSIS OF GRANULAR FABRIC EVOLUTION IN THREE-DIMENSIONS

ABSTRACT

Recent studies employing graph theoretic techniques from Complex Networks revealed the co-evolution of emergent minimal contact cycles
and load-bearing force chains as mesoscopic structures that form the basic
building blocks of self-organization. This study demonstrates previously observed trends for two-dimensional assemblages of circular discs to equally
apply when network analysis is applied to data from three-dimensional systems comprising non-spherical particles. As previously reported for two-
dimensional systems, the 3-cycles minimal contact cycle basis is both prevalent and persistent, providing support to force chains. In a new finding, the
majority of those 3-cycles are arranged so that they share a common contact
with the force chain column, transmitting nearly uniform normal contact
force magnitudes at the three contacts. Persistent 3-cycles in the sample are
absent in the region of strain localization in which force chains buckle, a finding that suggests a possible new structural indicator of failure and associated boundaries of flow.

REPORT DOCUMENTATION PAGE (SF298)
(Continuation Sheet)

Continuation for Block 13

ARO Report Number 51924.18-EV
A COMPLEX NETWORK ANALYSIS OF GRAN ...

Block 13: Supplementary Note

Approved for public release; distribution is unlimited.

To appear in
Dynamics of Continuous, Discrete and Impulsive Systems
http:monotone.uwaterloo.ca/∼journal

A COMPLEX NETWORK ANALYSIS OF GRANULAR FABRIC EVOLUTION IN THREE-DIMENSIONS

Antoinette Tordesillas[1], Sebastian Pucilowski[1], David M. Walker[1]
and
John Peters[2], Mark Hopkins[2]

[1]Department of Mathematics & Statistics
The University of Melbourne, Parkville, VIC 3010, Australia

[2]US Army Engineer Research & Development Center
Vicksburg, Mississippi 39180-6199, USA

Corresponding author email: jsmith@serve.uwaterloo.edu

Abstract. Recent studies employing graph theoretic techniques from Complex Networks revealed the co-evolution of emergent minimal contact cycles and load-bearing force chains as mesoscopic structures that form the basic building blocks of self-organization. This study demonstrates previously observed trends for two-dimensional assemblages of circular discs to equally apply when network analysis is applied to data from three-dimensional systems comprising non-spherical particles. As previously reported for two-dimensional systems, the 3-cycles minimal contact cycle basis is both prevalent and persistent, providing support to force chains. In a new finding, the majority of those 3-cycles are arranged so that they share a common contact with the force chain column, transmitting nearly uniform normal contact force magnitudes at the three contacts. Persistent 3-cycles in the sample are absent in the region of strain localization in which force chains buckle, a finding that suggests a possible new structural indicator of failure and associated boundaries of flow.

Keywords. Granular media, complex networks, particles, stability, discrete element method.

1 Introduction

We explore the efficacy of graph-theoretic tools and concepts from Complex Systems to uncover the evolution of fabric anisotropy (i.e., topology of internal connectivity) for an important class of discrete systems in three-dimensions: deforming assemblies of densely packed non-spherical grains under quasistatic loading. Attention is paid to problems of fundamental significance to geomechanics and, more broadly, to geotechnical engineering analysis and design. As with other complex systems, the behavior of granular soil under load is governed by the interactions among its constituent units

– in the case of granular systems the interactions occur between the constituent grains and between grains and the boundaries. These interactions give rise to known hallmarks of complexity including: behavior akin to phase transition and multiphase (solid-like to liquid-like) behavior, self-organized pattern formation (e.g., strain localization), and co-evolution of emergent internal structures (e.g., force cycles and force chains) [15, 24, 28, 44, 37]. With the advent of the Discrete Element Method (DEM), physical quantities that control these interactions, i.e., particle motion, contacts and contact forces, can all be measured in detail. Herein, we use data on these quantities from a DEM simulation of a triaxial test in [40] to demonstrate relatively new techniques for analyzing the evolution of fabric anisotropy in DEM-generated data sets for three-dimensional systems.

While there is abundant evidence on the impact of fabric anisotropy on granular soil behavior, a prevailing challenge lies in finding effective techniques for quantifying fabric anisotropy and its evolution. In the past, heterogeneities in the granular fabric have been quantified using statistical measures from spatial and frequency distributions of various fabric indicators. These include inter-particle contacts and associated voids, the magnitude and orientations of the contact vector (vector from center to point of contact), the branch vector (vector between centers of particles), and the long axis of non-circular particles [18, 22]. The question is: are there existing techniques from other areas, or can new techniques be devised, that would not only serve as a consummate detector of the fine details of contact topology but also provide a concise summary of fabric anisotropy and its evolution? This study is part of a broader effort initiated in [37, 42, 35, 33] to explore this question from the perspective of Complex Networks. Indeed one of the reasons for exploring the efficacy of graph-theoretic techniques which have been specifically designed for large graphs is to determine whether the resulting network properties can offer new insights into fabric and evolution of fabric anisotropy that would not otherwise be possible through any of the past techniques employed for fabric characterization.

In broad terms, virtually all complex systems are underpinned by one form of network or another (e.g., social, telecommunications, biological and electrical networks to name a few [21, 7, 4]). Identifying structures within these networks, particularly recurring patterns or motifs, and understanding how these co-evolve are crucial to the robust characterization and predictive modeling of these systems. A prevailing question in the broad area of complex networks, and one of prime interest in this investigation, concerns the connection between the properties of such networks and functional activity occurring in the system. Translated in the context of granular materials, we are thus interested in the connection between fabric on the one hand, and the nature of force transmission and the materials' ability to support load on the other. It is now of course well-established that contact and contact force networks govern the mechanical response or rheological behavior under load [14, 23]. Both have been studied extensively within the granular media community, but past efforts have not fully exploited the formalism of Complex Networks and only recently have there been attempts to characterize granular networks that arise in geomechanical settings. We refer readers to

a brief review in [42].

In a Complex Networks analysis, the deforming granular material is represented as an evolving mathematical graph or network in which the nodes or vertices represent the particles and the edges or links represent the contacts. In [37, 42, 35, 33], we have recently demonstrated how certain network features can succinctly capture and reveal previously unknown aspects of the deformation history in both space and time. A key outcome has been an improved understanding on functional activity at the mesoscopic scale: the role of self-organized columnar load-bearing force chains being stabilized by truss-like 3-cycles that provide both lateral support and rotational frustration at contacts. Three particles in mutual contact give rise to a 3-cycle: in Graph Theory this is a closed non-intersecting walk of path length equal to three (see also Figure 1) [42]. Although the techniques themselves are applicable to three-dimensional systems, these past studies have been confined to two-dimensions only. Of particular interest here is whether findings from circular particle assemblies, in two-dimensions, hold-up in three-dimensions especially in a system comprising non-spherical particles (e.g., poly-ellipsoids) – which are a more realistic archetype for analysis of real soils [16].

What is especially appealing about a networks perspective is that both the fabric and force transmission can be examined as one in the context of a weighted graph. We will examine two classes of sub-networks (or sub-graphs) in the global contact network of the system: (a) minimal cycles derived from the unweighted graph [37], and (b) the weighted graph where the links between the nodes are weighted by the magnitude of the normal contact force. Analysis of data from past discrete element simulations and photo-elastic disc experiments suggests that these subnetworks embody motifs [19], i.e., repeated sub-graphs that occur more frequently than expected in the contact network compared to an equivalent (same number of nodes and links) random graph, and that these motifs serve as basic building blocks for self-organization in dense granular systems. Quantifying the evolution of the properties of these sub-graphs should therefore shed light on the breakdown of functional connectivity and structure in the lead up to and during failure. Since failure patterns and boundaries of flow in three-dimensional specimens can be quite complicated and difficult to discern, we are particularly interested in structural forms that may provide useful indicators of boundaries separating failure (or flow-like regions) versus stable (solid-like) zones in the material.

The paper is organized as follows. In Section 2, we discuss salient aspects of the discrete element simulation in [40] – the source of the data to be used in the analysis. In Section 3, we define the various complex network properties that we will quantify and examine in relation to fabric evolution. In Section 4, we discuss the results of our complex analysis for the DEM simulation. We conclude in Section 5 with new lessons learned about the nature of fabric evolution and its connection to force transmission.

2 DEM Simulation

2.1 Micromechanics and Particle Shape

A large body of DEM work has been devoted to understanding the mechanical behavior of assemblages of circular discs, in two dimensions, and spheres in three dimensions, with a view toward deriving the general principles that control mechanical response of real materials (e.g.: [23, 13, 11, 32, 2]). Unfortunately, the link between trends observed in simulations of spherical particles and real granular media cannot be made without first resolving the role that rotation and its associated resistance play in particle kinematics. It has been noted that to get realistic behavior from discs and spheres, it is necessary to introduce significant rotational resistance to the contact interaction between particles [38, 26, 8, 10]. Non-spherical particles allow the simulation to capture rolling resistance without introducing the artifice of rolling resistance as a contact property. Although the surfaces of natural particles have some roughness, which creates resistance to rolling, the bulk of rolling resistance comes from non-spherical shapes. Depicting the rolling resistance as a contact property ignores important kinematical effects derived from the geometry of the particles within the mass. Thus, although the rolling resistance can be adjusted to create realistic simulations of bulk behavior with spherical particles, doing so has the cost of introducing uncertainties in the interpretation of the micromechanics. Spherical particles can rotate in place – without causing volume change whereas non-spherical particles cannot rotate without causing neighboring particles to displace thereby expanding the volume occupied by the particle group. Figure 1 illustrates this as well as highlights this fundamental difference in the context of 3-cycles which were recently found to co-evolve and serve as basic building blocks for self-organization with force chains.

The importance of volume change is in its contribution to the shear resistance of the particle group. At the continuum level, expansion of the bulk volume does work against the confining pressure providing resistance against shear, as embodied in the various classical stress-dilatancy laws of soil mechanics (e.g., [30]). At the scale of the particles, the volume expansion of non-spherical particle groups is tightly coupled to the particle rotations, which accordingly is strongly tied to force-chain buckling and formation of localized shear bands [24, 44, 33, 39]. It is indeed the case that volume change, particle rotation, force chain buckling, and shear-localization are all coupled in assemblages in spherical particles as well. Tordesillas et al [34, 9, 36] documented the process for the biaxial test in which force-chain buckling was treated as a process similar to the failure of a beam column in structural analysis. Rotation is a central part of the buckling mechanism, which is accompanied by asymmetrical lateral motion that opens void spaces causing dilation. For spherical particles the mechanics of particle buckling is controlled by contact resistance to rolling through an analogy between force chain buckling and elastic buckling of beam-columns. It is not clear that the beam-column analogy for instability of force chains holds up if significant *contact* resistance to rolling is absent. In the case of spheres, dilation caused

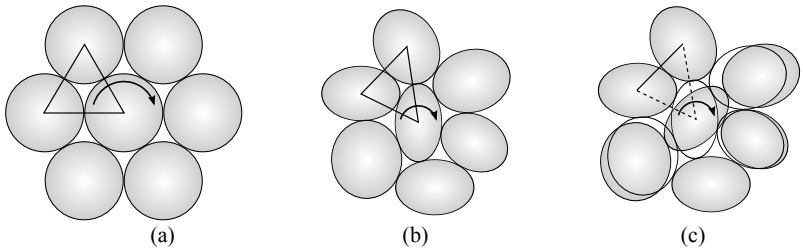

Figure 1: Volume expansion caused by rotation. (a) Rotation with local volume preserved for spherical particles, where the only impediment to rotations is the frustration offered by 3-cycle topology. (b) For non-spherical particles, dual resistance to rotation is provided by particle shape and 3-cycles. (c) Rotation enabled only through dilatant volume change *and loss of 3-cycles*.

by buckling is a secondary effect in which the resistance to lateral motion is mobilized *after* the instability condition is reached. The instability condition in columns of spheres is determined only by the stiffness of the rotational spring and the axial load through the force chain. For non-spherical particles, there is a direct coupling between volume change and rotation and the stability against buckling is derived from the complex motions within the particle group surrounding the force chain.

For the reasons expounded above, it follows that the formation of localized shear bands is closely tied to particle rotations. Thus, an overly idealized picture of how rotations are resisted ignores a major component of the micromechanical description of shear localization and brings into question the many insights derived for studies on spherical assemblages. The question in the present study is: do relationships between micromechanics and network descriptors identified in previous work hold up when network analysis is applied to presumably more realistic simulations involving non-spherical particles? The evident approach to determining how the coupled particle-group effect differs from simple contact rotation resistance is to perform analyses with non-spherical particles. Given analyses in three dimensions with particle shapes comparable to actual particles, the necessity of defending the simpler analyses with discs and spheres becomes unnecessary.

2.2 Numerical Simulation

The simulation used in the present network analysis is from the triaxial test studies performed in [40]. This was a successful study that compared simulations of triaxial tests to actual experiments and its thrust was to demonstrate a multiscale analysis in which direct experimental measurement of contact properties on binary pairs of particles [6] were used to calibrate the DEM model.

We now briefly discuss the salient details of this simulation starting from the particle shape used, followed by a summary of the sample preparation and material parameters. Readers are referred to [40, 6] for further details.

Poly-ellipsoids. The popularity of spherical particles in DEM studies of granular media mechanics derives from the simplicity of the contact detection algorithm [20]. Recent advances in use of ellipsoid and hyper-ellipsoids have expanded the options for simulation although these shapes have symmetries that potentially have subtle affects on micromechanics. The poly-ellipsoids, used in Uthus et al [40] and described in [27], remove particle symmetry while maintaining the simplicity of the ellipsoid. Each poly-ellipsoid is created by combining eight ellipsoidal patches to form a solid. The parameters defining each octant are chosen to ensure continuity in the surface and its gradient between octants, thus creating the smooth pebble-like shapes shown in Figure 2. An equivalent description of the particle shape is as a deformed ellipsoid in which the equatorial radii have different values in the positive and negative directions.

Sample preparation and material parameters. The simulation was based on the standard stress driven triaxial test. The cylindrical specimen consisted of poly-ellipsoid particles encased within a flexible membrane and loaded between two rigid end-platens. Because the flexible membrane constituted an irregular outer boundary, porosity was computed by a simple Monte Carlo integration whereby the core of the cylinder was randomly sampled with 1 million points and the fraction of particles falling outside a particle approximated the porosity. During both hydrostatic consolidation and subsequent application of the deviator stress, the location of the top platen was held constant, while the bottom platen was pushed upward. In Figure 3 we show a rendering of the poly-ellipsoid assembly at three simulation time steps throughout loading: the initial configuration of the particles; a snapshot of the evolving assembly during the early stages of loading; and the configuration of the assembly at the final stage of loading. The confining membrane of the triaxial test is not shown so as to expose the particles. A Hertzian normal and tangential contact force model was used. A summary of the simulation parameters is given in Table 1. We observe for the evolving and final configuration the bulging of the material indicative of the onset and persistence of failure zones.

Figure 4 presents the strain evolution of the deviator stress and volumetric strain for the sample. Of particular interest in the present study is what contact network structures and properties can be used to complement these and those measurements reported in [40] in order to help characterize and ultimately predict such failure zones.

3 Complex Network Methods

In this section, we briefly introduce a selection of pertinent concepts from Complex Networks which we have found to be particularly useful for quantifying the evolution of granular fabric in 2D systems. The intent then is to apply these to quantify the evolution of granular fabric in a 3D assembly of poly-ellipsoids subject to triaxial compression using data from [40]. To this end, we consider the assembly of granular particles as a complex network with the vertices (or nodes) representing the particles and the links (or

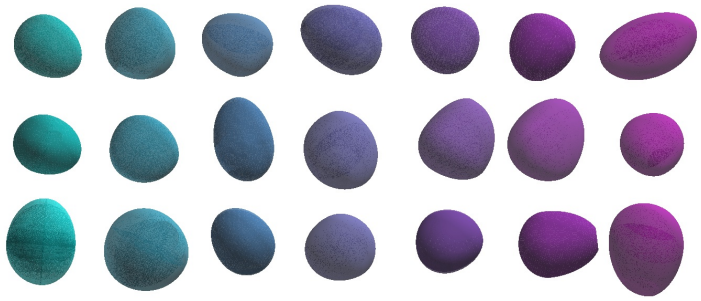

Figure 2: Varying pebble-like shapes produced by poly-ellipsoids.

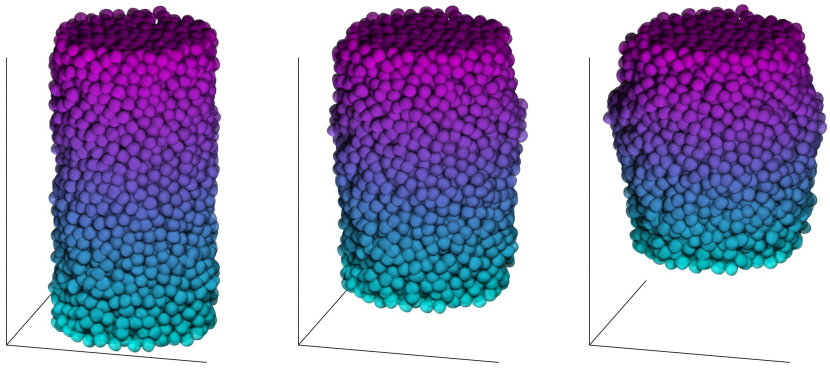

Figure 3: Initial distribution of particles (left), evolving (middle) and final configuration (right). Color scale indicates initial elevation of particle.

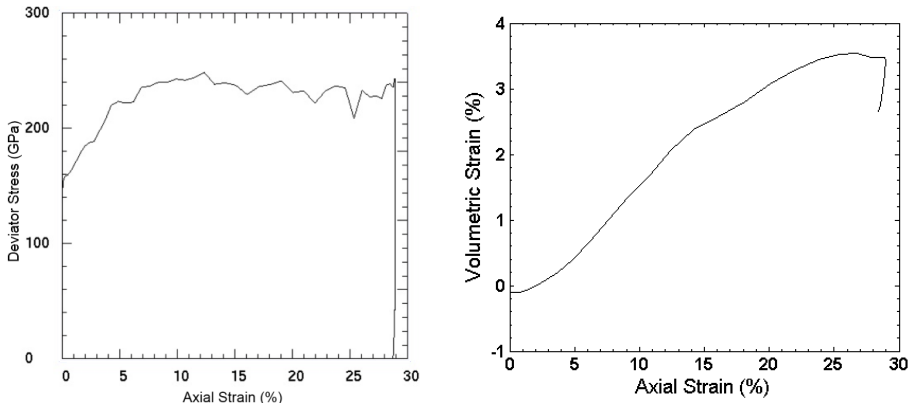

Figure 4: Strain evolution of the deviator stress (left) and volumetric strain (right) from the simulated triaxial test.

Parameter	Value
Confining pressure	140 kPa
Time-step increment	1×10^{-6} s
Number of particles	3456
Initial porosity	0.35
Particle density	2600 kg/m^3
Shear modulus G	30 GPa
Poisson ratio	0.3
Minimum particle radius	1.76×10^{-3} m
Average particle radius	2.60×10^{-3} m
Maximum particle radius	4.57×10^{-3} m
Initial specimen height	1.25×10^{-1} m
Initial specimen diameter	6.68×10^{-2} m
Final specimen height	9.10×10^{-2} m
Interparticle friction μ	0.28 (damped)
Particle-wall friction μ	0.28 (damped)
Normal spring stiffness k^n	Variable Hertzian
Tangential spring stiffness k^t	Variable Hertzian

Table 1: DEM simulation and material parameters.

edges) between nodes exist if the corresponding particles are in physical contact. As the material deforms and self-organizes in response to the applied loading, old contacts are broken and new contacts are formed, resulting in an evolving complex network. In the present study, we have 3456 particles in our assembly, and so each contact network for a given strain state consists of 3456 nodes and the connectivity of the packing typically consists of approximately 24000 links. These networks can be summarized by a collection of network statistics [21, 7, 4] and the changing behavior of the material manifests itself in the evolution of such measures [42]. Typical network statistics include a description of network clustering coefficients that summarize the connectivity and any propensity of the material to favor locally dense configurations even under global dilatation – beyond a simple count of the number of contacts per particle. Thus the evolution of the granular fabric can be quantitatively characterized from these statistical properties. Specifically, the emergence of specific mesoscopic structures within the network, especially those that are both prevalent and persistent, can be identified and related to known rheologically important physical structures such as force chains and their lateral support. These structures are termed "network motifs" [19]. Here we pay particular attention to low-order cycles, in particular the 3-cycles of a minimal cycle basis that were previously found to be of great importance in 2D systems [42, 37, 35, 33].

A study of the evolving structure of the materials' contact network involves the *unweighted complex network* which is mathematically summarized by an unweighted adjacency matrix $\mathbf{A}$ whose non-zero elements a_{ij} are such that $a_{ij} = 1$ if particles i and j are in contact. Thus such a study is solely focussed

on connectivity. However, the topology of a granular contact network can be further enriched to include information on other aspects of particle interactions by weighting each network link with a physically meaningful quantity — the most obvious being that of the contact force. In our present study, we consider the case when the weight assigned to each link is the magnitude of the normal contact force, since this has been found to govern the shear strength of dense granular materials (tangential contact forces are typically an order of magnitude smaller) [2]. This leads to an investigation of a *weighted complex network* that is summarized by a weight matrix $\mathbf{W}$, with the non-zero element w_{ij} representing the magnitude of the normal contact force (instead of $a_{ij} = 1$ in the unweighted adjacency matrix). Analysis of this weighted matrix $\mathbf{W}$, instead of $\mathbf{A}$, leads to generalizations of the unweighted statistics, namely, vertex strength, a weighted clustering coefficient and sub-graph coherence.

3.1 Vertex degree

In an unweighted complex network, one of the most fundamental properties is the degree of a vertex (or node) and the degree distribution. The vertex degree is the number of links it has, or the number of particles it is in contact with in a contact network, and is easily calculated using the adjacency matrix:

$$k_i = \sum_j a_{ij} \tag{1}$$

The degree for each particle can be averaged over all particles to obtain a measure that is commonly known as the coordination number within the granular media community [1]. For granular systems, this quantity remains a popular rheological property both in the physics and engineering communities: see, for example, [41, 29]. However, this measure does not distinguish the heterogeneities in the topology of contacts around a particle. Measures that do account for such heterogeneities are clustering coefficients

3.2 Clustering coefficient and minimal cycles

A second useful and informative quantity of a network is the clustering coefficient [21, 43, 31]. The clustering coefficient quantifies the local connectivity of a node by measuring the number of triangle motifs, closed paths of length three, i.e., 3-cycles, associated with it and its contacting neighbors. It can be explicitly calculated using the entries, a_{ij}, of the adjacency matrix [4]:

$$c(i) = \frac{1}{k_i(k_i-1)} \sum_{j,h \in V(i)} a_{ij}a_{jh}a_{hi}, \tag{2}$$

where k_i is the vertex degree defined above and $V(i)$ is the set of neighboring vertices of i. As with degree each $c(i)$ can be averaged over all particles to obtain a macroscopic summary of the 3-cycles in the network. The clustering coefficient ranges from 0 (none of a particle's contacting neighbors

have contacts between them) to 1 (all of a particle's contacting neighbors are fully connected to each other).High values of $c(i)$ corresponds to a local closely packed structure and hence to potentially more stable areas within the material, especially as triangular arrangements of particles frustrate rotations [37, 35, 33].
The clustering coefficient presented here is the most standard and simplest one to quantify 3-cycles in a network. More general clustering coefficients have been proposed in the complex network literature. For example, Lind et al [12] introduce a clustering coefficient to quantify the amount of 4-cycles in a network. However, since the size of the contact networks studied here are relatively small it is feasible to calculate a *minimal cycle basis* which explicitly considers all n-cycle populations and their evolution [37].
A minimal cycle basis of a graph is a set containing the shortest cycles, i.e., cycles with minimum length or number of edges, and can be calculated using an algorithm described in [17]. Readers are referred to [5] for more details on n-cycles in an undirected graph: a closed path or a non-intersecting walk of length n where $n \geq 3$ with no repeated vertices other than its initial and final vertex. In [37], we showed how the strain evolution of the minimal cycle basis of the contact network can be used to describe the progressive loss of connectivity in the sample as well as the development of dilatation.

3.3 Vertex strength

By overlaying the topology of contacts with contact force information through analysis of the weighted complex network $\mathbf{W}$, we can extend the notion of particle or vertex degree to vertex strength [4]:

$$s_i = \sum_{j \in V(i)} w_{ij}, \tag{3}$$

where $V(i)$ is the set of neighboring vertices of i and w_{ij} is the weight of the contact link ij. The strength of a vertex carries information both about its local connectivity and the importance of the weights of its contacts links. It can be considered as a natural generalization of connectivity. Any scalar can be chosen to weight the network; here we have chosen the normal contact force magnitude.

3.4 Weighted clustering coefficient

The weighted clustering coefficient is:

$$c^w(i) = \frac{1}{s_i(k_i - 1)} \sum_{j,h \in V(i)} \frac{(w_{ij} + w_{ih})}{2} a_{ij} a_{jh} a_{hi}, \tag{4}$$

where s_i is the strength of vertex i defined previously, k_i is the vertex degree, $V(i)$ is the set of neighboring vertices of i, w_{ij} is the weight of link ij and a_{ij} is 1 if a link exists between ij, and 0 otherwise, i.e., an element of the network adjacency matrix [4]. This takes into account the influence of weight

(normal contact force magnitude) distribution of the network, in addition to the local connectivity. In this way, the local topology of 3-cycles can be ranked in terms of the strength of their connections as well as their local abundance, i.e., 3-cycles carrying high normal contact force at their contacts will contribute to a higher $c^w(i)$ coefficient.

3.5 Sub-graph coherence

The sub-graph coherence $Q(G)$ of a local sub-graph G within the network is the ratio of the geometric mean to the arithmetic mean of the link weights of the sub-graph:

$$Q(G) = \frac{|l_G| \left(\prod_{(ij) \in l_G} w_{ij} \right)^{1/|l_G|}}{\sum_{(ij) \in l_G} w_{ij}}, \tag{5}$$

where l_G are the links in the sub-graph, $|l_G|$ are the number of links and w_{ij} is the weight of link ij [4, 25]. This measure takes values in $[0, 1]$. A value close to 0 implies that the weights differ greatly, whereas values close to 1 indicates the weights are internally similar (or close to being uniformly distributed) . Note, the coherence does not distinguish between high or low contact forces being internally consistent, only that the contact forces within the sub-graph in question are internally similar.

4 Results

Before we discuss the results of the Complex Network analysis, some familiarity with the deformation pattern of the sample is useful. Three distinct zones developed during the deformation (see, Figure 5). Next to the top platen which is kept fixed, we find a zone of un-deforming material (a so-called 'dead zone') in the shape of a blunt solid cone wherein particles undergo negligible motion throughout loading. A similar conical region of un-deforming material develops at the bottom of the sample: this region moves in essentially rigid body motion with the upward moving bottom platen. In between lies a region of localization where buckling force chains reside. This region, which caps the dead zones, bulges outwards in the middle with particles moving laterally due to dilatation. Note the frequency distribution of the displacement magnitudes in Figure 6 shows peaks at the opposite extremes: the particles associated with these peaks are those in the top and bottom dead zones of Figure 5.

A key focus of this study is the load-carrying capacity (or shear strength) of the sample and its relation to the internal connectivity (or fabric). The former is typically quantified in a triaxial test by the ratio of the deviator stress to the mean stress. It has been shown that contacts which bear above-the-global-average normal contact force are the main contributors to the deviator

stress ratio [3]. The global average normal contact force is thus a good indicator of the load-carrying capacity or shear strength of the material. Two related network properties of the weighted and unweighted contact network, i.e., vertex strength and degree, quantifies the evolution of shear strength and connectivity: see Figure 7. Beyond the peak, and modulo fluctuations, the material undergoes an essentially monotonic but relatively slow rate of decrease in its shear strength compared to the rate of change prior to peak. Thus the vertex strength of a weighted complex network with weights given by the magnitude of the normal contact forces may provide a good proxy for the deviator stress of the material.

The strain evolution of the global average degree (inset of Figure 7, closely related to coordination number) reveals a progressive loss of connectivity in the system, with the most rapid decline occurring early in the loading history before axial strain of 15%. This is suggestive of responsive rearrangements resulting in rapid dilatation during these stages of the loading history.

Whereas degree is an obvious starting point for any quantification of connectivity, it does not account for the heterogeneities in the contact arrangements around a particle. The same can be said of the local porosity, the ratio of void volume to total volume, which is also commonly used in the granular mechanics literature. In the past, such heterogeneities have been quantified, usually on the global scale, via statistical properties derived from histograms of the orientations of key fabric indicators; among these are the contact vector (vector from center to point of contact), the branch vector (vector between centers of particles), and the long axis of the particle (if it is noncircular) etc. The question is: can we do better? Can we devise new or use existing techniques from other areas that would not only serve as a consummate detector of the fine details of contact topology but also provide a concise summary of fabric anisotropy and its evolution.

In past studies, focusing on circular particles in two dimensional DEM simulations with "rolling resistance" included to account for particle shape, complex network techniques proved very effective and uncovered previously unknown details of the co-evolution of load-bearing force chains and the stability offered by their supporting minimal contact cycles [37, 33]. We now show in Figure 8, the member populations of the minimal cycle basis of the contact network (combined population of large n-cycles, $n > 5$, is less than 0.03% of total and is not shown in the plot). The 3-cycles constitute the clear majority throughout loading. More importantly, the connection between connectivity and strength of the material is evident in the 3-cycle membership. During the first half of the loading history (period before axial strain of 15%) a progressive decline in both the total population of 3-cycles (Figure 8) and the average per particle density of these structures as measured by the clustering coefficient in the unweighted and weighted networks (Figure 9). Recall, the weighted networks include the additional information of normal contact force magnitude. In this case, the global average of the weighted information does not appear to give additional insights to the unweighted version, however, as we discuss later consideration of weighted networks is valuable. The highest attrition rate for 3-cycles occurs prior to axial strain of 15% (Figure 8 and Figure 9). This coincides with increases in the 4-cycle and 5-cycle pop-

ulations, that is, a complex network signature of dilatancy is the breaking of 3-cycle topologies to form higher length cycles (recall the illustrations of Figure 1). In two-dimensions, the same qualitative trends were observed for dense assemblies; indeed, where a granular contact network forms a planar graph (2D), this finding is consistent with Euler's formula relating nodes (particles), links (contacts) and faces (cycles) [35].

Evidence from various simulations and photo-elastic disc experiments, in two dimensions, suggest that force chains reside in local topologies with a relatively higher density of connections in 3-cycle formations, i.e., higher degree and higher clustering coefficient [37, 42, 35, 33]. Here we also find that particles in force chains do indeed have a higher degree and a higher number of 3-cycles per particle (Figure 10). This relationship between 3-cycles and force chains corroborates earlier results in two-dimensional systems which revealed the stabilizing role that these structures provide to load-bearing columnar force chains. Interestingly, the strong columnar particle structures that we call force chains lie mainly in the upper regions of the sample, percolating from the middle strain localization region through to the fixed boundary at the top. The lower portion of the sample, while inhabited by strong contacts bearing above-the-global-average contact forces, does not embody strongly-loaded chains of particles (greater than three) in quasi-linear formation; see Appendix for our definition and method of detection of force chains.

We now turn our attention to the force distributions in the important 3-cycles which requires the consideration of weighted networks. We quantify this using the network property of coherence (see Equation (5)), a measure of how similar the three contact force magnitudes are in each 3-cycle: equal force magnitudes in a 3-cycle correspond to the highest value of coherence of 1 for that cycle. In general, we find 3-cycles to have low coherence (less than 0.3) (see Figure 11) signifying large variations in the magnitudes of the forces they carry. For example, those 3-cycles conjoined with force chains never exceed a global average coherence of 0.25. Interestingly, there is a small contingent of the 3-cycle population, the 3-force-cycles, which bear a disproportionately high level of coherence (above 0.9) (see, Figure 11). In a previous study, 3-force-cycles, which are 3-cycles whose constituent contacts *each* bear above-the-global-average normal contact force, were found to grow in numbers inside the shear band during the development of the shear band, i.e., from initiation to the fully developed shear band or start of the critical state regime [37]. In the current simulation, throughout loading, we found typically 95% of 3-force-cycles existed within the strain localization region. Thus, the rules governing self-organization of 3-force-cycles within a deforming dense two-dimensional assembly of circular particles (with rolling resistance or contact moment introduced at the contacts) appears to generalize to three-dimensional dense poly-ellipsoid assemblies [37, 35, 33].

The connection between 3-cycles and force chains can be explored in further detail. Figure 12a illustrates two topological configurations by which 3-cycles offer support to force chains: (Mode I) the 3-cycle shares an edge/contact with a force chain or (Mode II) the 3-cycle shares a vertex/particle with a force chain. The relative populations of these modes for 3-cycles conjoined with force chains is presented in Figure 13. Mode I is the governing majority

for the 3-cycles, nearly 80% of all conjoined 3-cycles have this configuration. The high incidence of Mode I 3-cycles is similarly reflected in the low 3-cycle coherence (Figure 11). For 3-force-cycles, the relative populations vary more so, but the majority support structure is still Mode I, typically 60% − 75%. In this case, since 3-force-cycles are more coherent structures, the two supporting contacts and the contact along the force chain are close to being of equal magnitudes (recall Figure 11). That is, 3-force-cycles give greater lateral support to force chains, and the material appears to be preferentially rearranging to promote the existence of such structures.

Motivated by the relevance of 3-cycles in connection with force chains, we next examined the lifetime distributions of these supporting structures (Figure 14). We define the lifetime of a structure to be the number of consecutive (observed) strain stages the structure remains intact, i.e., from inception to termination. On average, 3-cycles persist for around 5% axial strain. What is most interesting is that we find a fraction of the initial 3-cycles survive throughout the loading history. These persistent 3-cycles, existing throughout loading from start to end, lie in regions *outside of the strain localization zone where the buckling force chains form*: see Figure 15. The same trend has been observed in two-dimensional systems which suggests that the absence of these 3-cycles that exist throughout loading in certain regions of the specimen may be indicative of regions of strain localization.

Finally, for three-dimensional systems, it is also of interest to probe structures made up of 3-cycles, e.g., tetrahedral motifs. Tetrahedra consist of an agglomeration of 3-cycles which all share edges, and can only occur in three-dimensional systems. The strain evolution of tetrahedral structures exhibit similar trends to those observed for 3-cycles as shown earlier in Figure 8. As exemplified in Figure 12b, the local contact topology of columnar structures like force chains is often rich in 3-cycles and tetrahedral motifs both at the sides for lateral support and capped at the ends for additional support.

5 Conclusion

The evolution of granular fabric and that of force transmission are key to a robust characterization and predictive modeling of granular materials. Herein we presented the first attempt at quantifying each of these and importantly their interconnection using graph-theoretic techniques from Complex Networks for a three-dimensional DEM simulation of an assembly of poly-ellipsoidal particles under monotonic triaxial compression. Following earlier studies undertaken by [37, 42, 33], we focussed on recurring patterns in the contact and contact force networks. We uncovered similarities with two dimensional systems, particularly with respect to the co-evolution of basic building blocks for self-organization, i.e., 3-cycles and force chains. The 3-cycles constitute the clear majority in the minimal cycle basis throughout loading with the highest attrition rate for these occurring in the early stages of loading. Force chains reside in local topologies with a relatively higher density of connections in 3-cycle formations. This association between force chains and 3-cycles corroborates earlier results in two-dimensional systems which revealed the

same trend and the *dual stabilizing* role that 3-cycles provide to load-bearing columnar force chains which are prone to buckling (i.e., 3-cycles prop-up force chains and frustrate particle rotation).
We uncovered new insights into the salient aspects of topology and lifetimes of these building blocks. Topological configurations by which 3-cycles offer support to force chains reveal the majority are arranged such that a 3-cycle shares an edge (i.e., a contact) with a force chain, as opposed to a shared vertex (i.e., a particle) with a force chain. This contact sharing is a critical piece of information in the Structural Mechanics modeling of confined buckling of force chains (e.g., [34] and [9]). We also examined 3-force-cycles, a subset of the 3-cycles distinguished from the rest by the strength of their contacts: each contact in a 3-force-cycle carries above-the-global-average normal contact force. We observed that these strong 3-cycles are close to being uniform: the normal contact forces are of similar magnitude over all the three contacts. A major new insight revealed that the lifetime distributions of these supporting 3-cycles contained persistent 3-cycles, i.e., 3-cycle motifs which exist from the start to the end of loading. The location of such persistent structures showed they lie in the regions *outside* of the strain localization zone where the buckling force chains form. This trend suggests that the absence of such long-lived 3-cycles in certain regions of the specimen may be indicative of strain localization in these locations. Apart from these long-lived 3-cycles, the rest of the 3-cycles in this specimen lived for an average strain interval of around 5% axial strain. Tetrahedral structures (a combination of four 3-cycles) exhibit similar trends to those observed for 3-cycles, and force chains benefit from the lateral support of both 3-cycles and tetrahedra at the sides and being capped at their ends.
It is to be expected that the trends in the network descriptors reported here depend on loading conditions, particle shape and material properties. Nevertheless, that these results share many common features with those earlier reported for two-dimensional assemblies demonstrate that the co-evolution of linear and cyclic motifs in the contact and contact force networks of dense granular systems warrant continued investigation. This study has also revealed details of granular fabric that have not been previously reported in past studies of three-dimensional systems.

Appendix

5.1 Finding Force Chains

This section presents a quantitative algorithm for finding force chains within a granular assembly. Here we use an approach in which a force moment tensor for a particle is calculated as follows:

$$\hat{\sigma}_{ij} = \sum_{c=1}^{N} f_i^c r_j^c,$$

where N is the number of contacting neighbors of the particle, f_i^c denotes the components of the contact force and r_j^c denotes the components of the unit

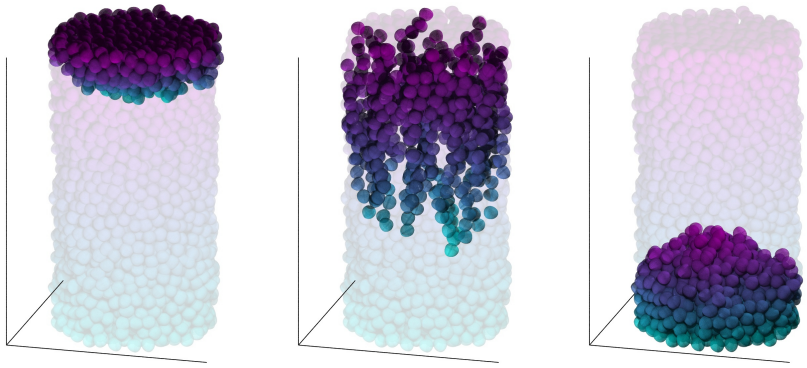

Figure 5: Three regions identified: two undeforming regions (left/right) mediated by a strain-localization region where buckling force chains reside (middle).

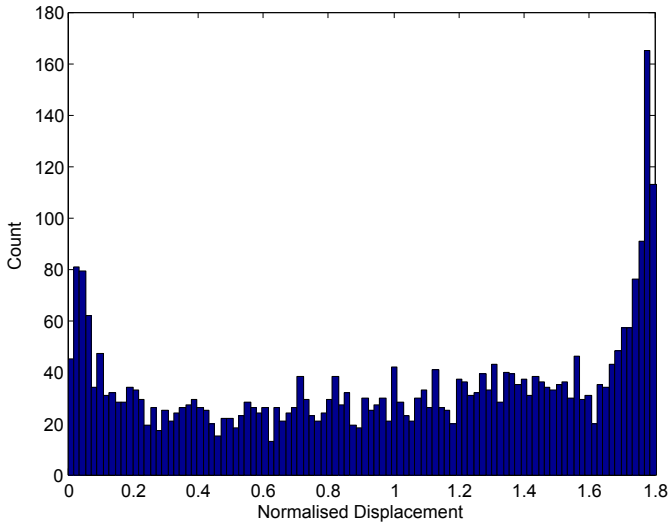

Figure 6: Normalized displacement magnitude frequency count. The top and bottom undeforming regions in the sample lie in the top and bottom 20% of particle displacement magnitudes, respectively.

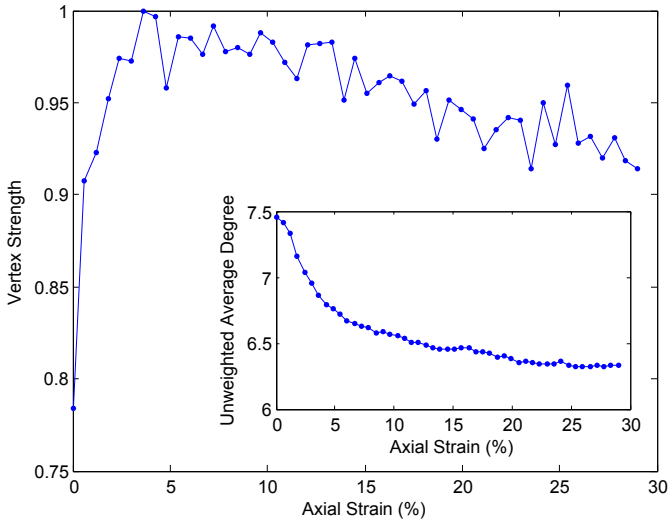

Figure 7: Mean vertex strength normalized against peak value throughout the loading history. (inset) Unweighted mean degree throughout the loading history.

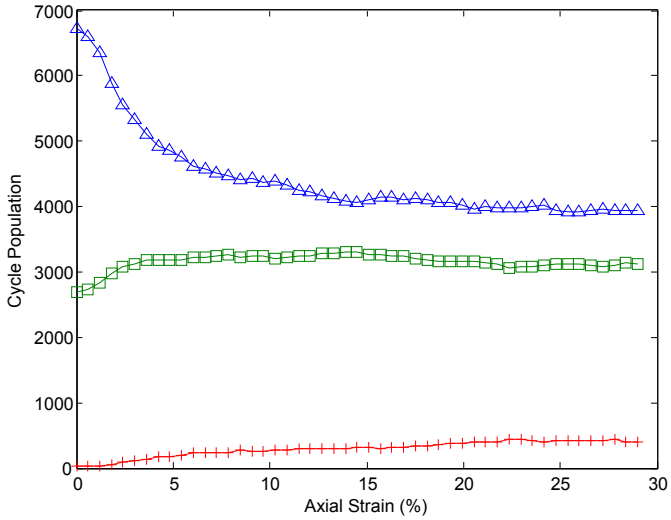

Figure 8: Cycle populations throughout loading. △ denote 3-cycles, □ denote 4-cycles, + denote 5-cycles. Higher order cycles have negligible populations.

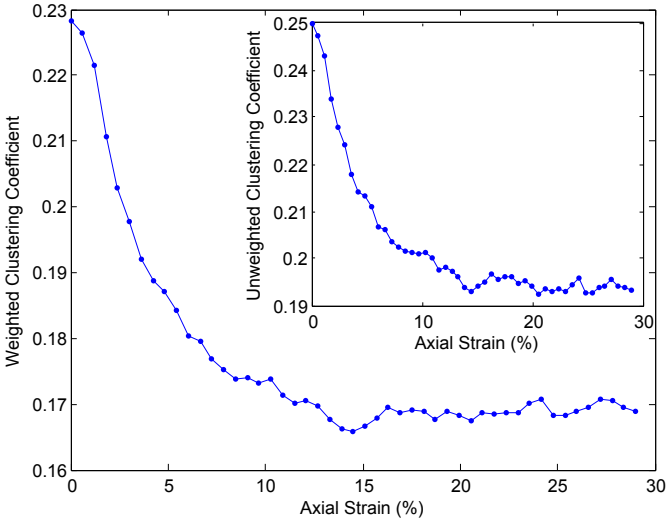

Figure 9: Weighted mean clustering coefficient throughout loading history. (inset) Unweighted mean clustering coefficient throughout loading history.

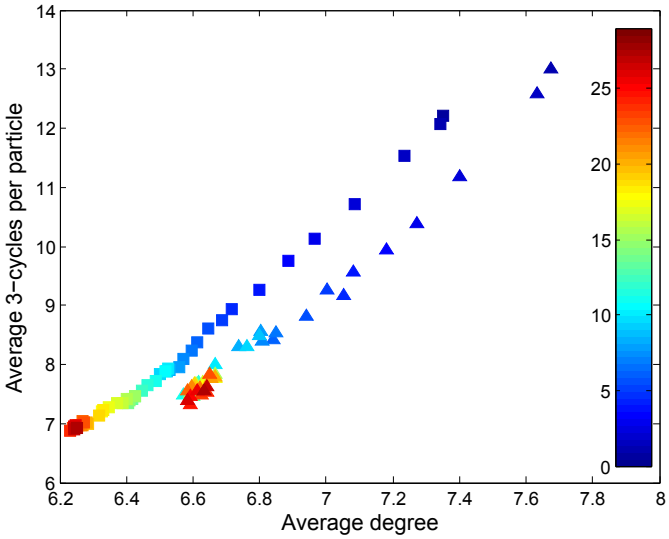

Figure 10: Feature vector showing the strain evolution of the number of contacts and 3-cycles per particle in two subsets: those in force chains (△) versus the rest □. Legend indicates simulation stage.

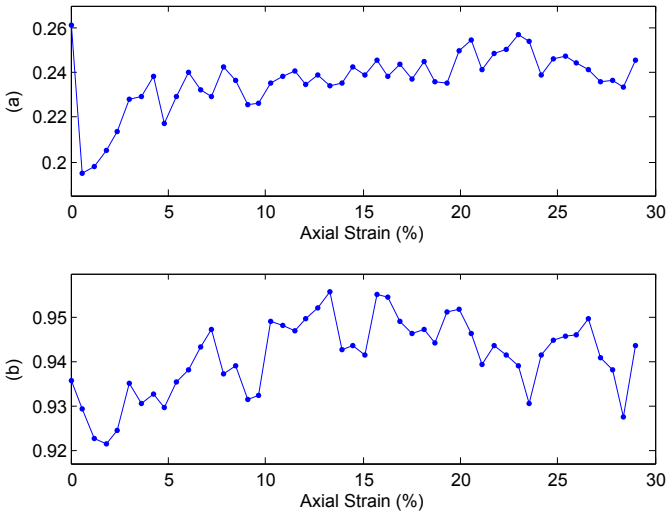

Figure 11: Mean coherence throughout loading history of 3-cycles conjoined with force chains: all 3-cycles (top) and 3-force-cycles (bottom).

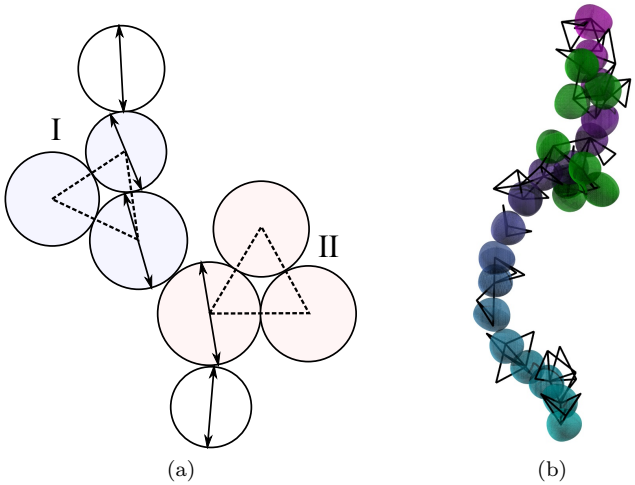

Figure 12: (a) Contact topologies of 3-cycles conjoined with force chains (particles with double arrows): 3-cycle shares an edge with a force chain (Mode I) and a 3-cycle shares a vertex with a force chain (Mode II). (b) A force chain and its supporting structures. 3-cycles and tetrahedral supports are shown, with the particles colored green being those in the tetrahedral clusters.

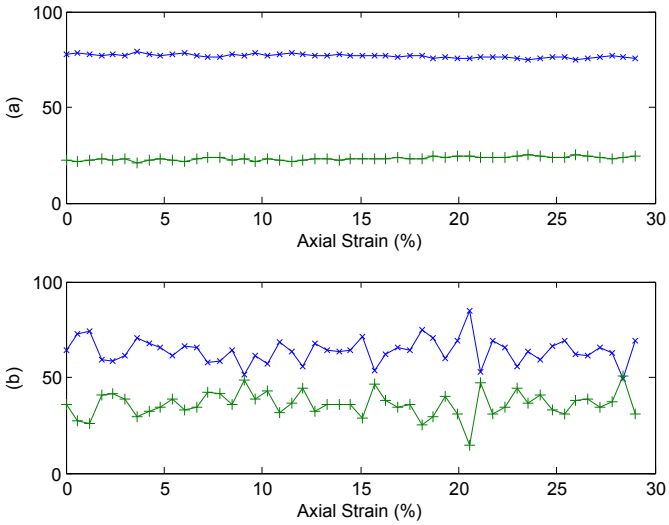

Figure 13: Percentages of 3-cycles around force chains in Mode I (×) versus Mode II (+) configurations throughout loading history: all 3-cycles (a) and 3-force-cycles (b).

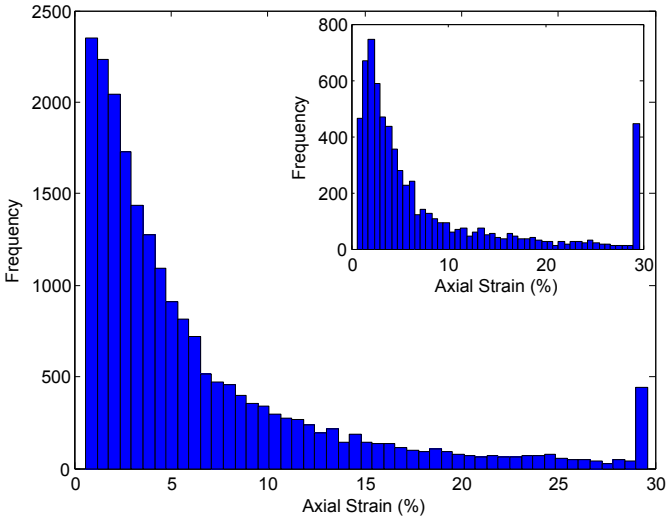

Figure 14: Frequency distribution of the ages of all 3-cycles created throughout loading history. The inset shows the frequency distribution of the ages of all the 3-cycles that were present at the start of loading; the peak at the final strain interval corresponds to the *persistent* 3-*cycles* which lived throughout loading history.

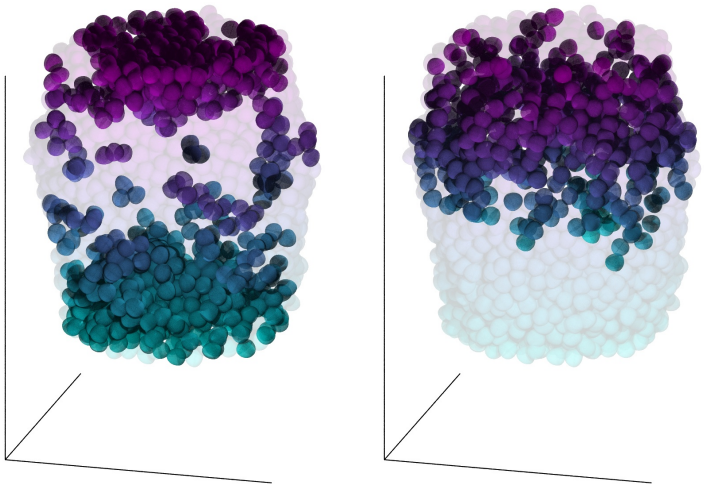

Figure 15: Persistent 3-cycles (left) and all buckling force chains (right). The former comprises 3-cycles which exist from start to end of loading; the latter image shows the accumulated population of all buckled force chains.

normal vector from the center of the particle to the point of contact. The largest eigenvalue of the force moment tensor and its associated eigenvector define, respectively, the magnitude and direction of the *particle load vector* $\mathbf{P}$ (PLV).

Sequences of contacting particles exceeding three or more whose load vectors align within a prescribed tolerance angle, and whose magnitude is above average, embody a force chain.

Particles with no contacting neighbors are removed from candidacy. For each remaining particle in the system, we calculate its force moment tensor and corresponding PLV as above. The mean PLV magnitude is calculated for the remaining assembly. Particles whose magnitude fall below this value are filtered out; the remaining are candidate particles for force chains.

The particle with the largest PLV magnitude is selected as the start of a force chain. Neighboring candidate particles are considered, and we look in the direction of the PLV.

We define a tolerance angle θ° that is used to search for contacts. A θ° value of 0 corresponds to perfectly linear force chains, which is unrealistic. A θ° value of 45° allows force chains a realistic amount of curvature. Hence our *quasi-linearity* condition is:

$$\cos\theta < \frac{\mathbf{P}\cdot\mathbf{l}_c}{|\mathbf{P}||\mathbf{l}_c|} \leq 1.$$

where $\mathbf{l}_c$ is the branch vector from the center of the particle to the neighboring candidate.

This means any neighboring candidate must lie within a θ° cone with apex centered at the particle center – in 2D this reduces to a sector.

A situation may occur where although a candidate lies within the allowed region, the reverse may not be true. To prevent this, a *back check* is performed where the same constraint as above is used, but with the particles switched, that is:

$$\cos\theta < \frac{\mathbf{P}' \cdot \mathbf{l}_c}{|\mathbf{P}'||\mathbf{l}_c|} \leq 1.$$

where $\mathbf{P}'$ is the candidate particles' PLV (see, Figure 16).
If a number of valid choices passing the above condition exist for choosing the next particle to be added to a force chain, a heuristic may be employed. One may select a particle with highest PLV magnitude, or one which encourages the formation of longest or straightest creation of force chains.
Once a match is selected, it is added to the chain and the process is repeated until the chain cannot grow further. We then return to the initial force chain particle, and search *backwards* in a similar fashion.
Particles found in the above iteration are removed from candidacy. If more than two were found, we call this collection of particles a *force chain*. The above repeats until no more candidate particles exist.

5.2 Buckling Force Chains

A force chain can be regarded as failing, or beginning to fail, if it experiences a drop in load carrying capacity and structurally fails. We call such force chains *buckling force chains* [37].
A strain interval is selected to test if previously found force chains buckled during this intervening time. The particle load vector magnitude of all particles of a force chain (excluding head and tail) are compared over this interval. If a particle experiences a drop in particle load vector magnitude, we check its buckling angle (Figure 17). If this angle exceeds a prescribed threshold $\theta_t < |\theta_i - \theta_f|$, then the *entire* force chain is classified as buckled.

Acknowledgments

This work was supported by US Army Research Office (W911NF-07-1-0370) and the Australian Research Council (DP0986876 and DP0772409). We also thank the Victorian Partnership for Advanced Computing for computing resources.

References

[1] I. Agnolin and J.-N. Roux. Internal states of model isotropic granular packings. i. assembling process, geometry and contact networks. *Physical Review E*, 76:061302, 2007.

[2] S. J. Antony. Link between single-particle properties and macroscopic properties in particulate assemblies: role of structures within structures. *Philosophical Transactions of the Royal Society A*, 365(1861):2879–2891, 2007.

[3] S. J. Antony and M. R. Kuhn. Influence of particle shape on granular contact signatures and shear strength: new insights from simulations. *International Journal of Solids and Structures*, 41:5863–5870, 2004.

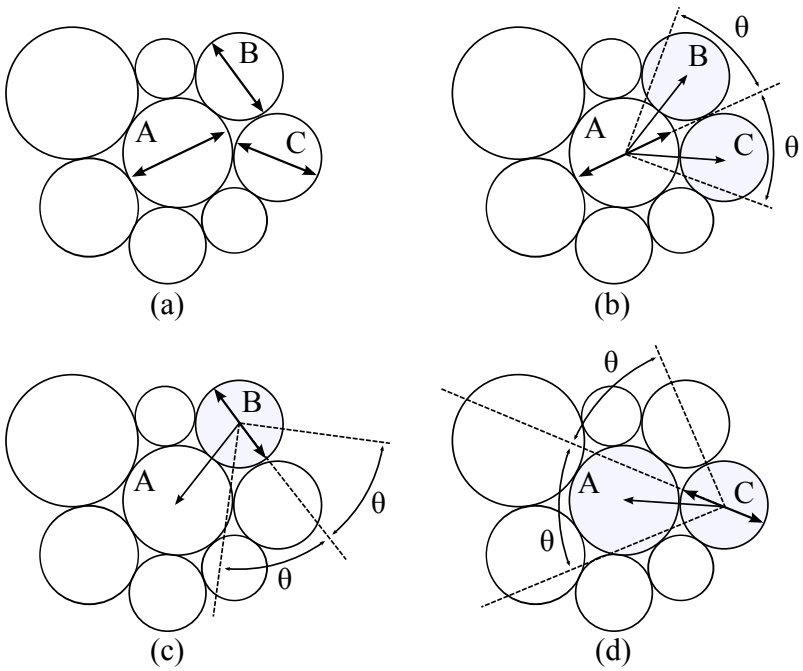

Figure 16: Algorithm for finding force chains. Double-sided arrows through particle centers denote the direction of the particle load vector. Single-sided arrows joining particle centers denote branch vectors. (a) Particle with highest particle load vector magnitude is selected, A. (b) Look forward in the direction of the particle load vector for contacts inside tolerance angle, B and C. (c) Select B and perform a back check. Since A does not lie within the tolerance angle, B is rejected. (d) Select C and perform a back check. A lies within the tolerance angle, so the back check is successful and C is the next particle in the chain.

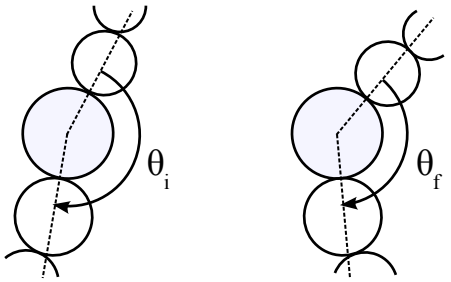

Figure 17: The highlighted particle experiences a drop in particle load vector magnitude during some specified interval. If the change in angle exceeds some threshold, $\theta_t < |\theta_i - \theta_f|$, then the *entire* force chain is classified as buckling.

[4] S. Boccaletti, V. Latora, Y. Moreno, M. Chavez, and D.-U. Hwang. Complex networks: structure and dynamics. *Physics Reports*, 424:175–308, 2006.

[5] B. Bollobás. *Modern Graph Theory*. Springer, 1998.

[6] D. M. Cole and J. F. Peters. A physically based approach to granular media mechanics: Grain-scale experiments, initial results and numerical modeling. *Granular Matter*, 9:309–321, 2007.

[7] L. da F. Costa, F. A. Rodrigues, G. Travieso, and P. R. Villas Boas. Characterization of complex networks: a survey of measurements. *Advances in Physics*, 56(1):167–242, 2007.

[8] Nicolas Estrada, Alfredo Taboada, and Farhang Radjaï. Shear strength and force transmission in granular media with rolling resistance. *Physical Review E*, 78:021301, 2008.

[9] G. W. Hunt, A. Tordesillas, S. C. Green, and J. Shi. Force-chain buckling in granular media: a structural mechanics perspective. *Philosophical Transactions Of The Royal Society A*, 368:249–262, 2010.

[10] M. J. Jiang, H.-S. Yu, and D. Harris. A novel discrete model for granular material incorporating rolling resistance. *Comput. Geotech.*, 32(5):340–357, 2005.

[11] N. P. Kruyt and L. Rothenburg. Shear strength, dilatancy, energy and dissipation in quasi-static deformation of granular materials. *Journal of Statistical Mechanics: Theory and Experiment*, page P07021, 2006.

[12] P. G. Lind, M. C. González, and H. J. Herrmann. Cycles and clustering in bipartite networks. *Physical Review E*, 72:056127, 2005.

[13] S. Luding, M. Lätzel, W. Volk, S. Diebels, and H.J. Herrmann. From discrete element simulations to a continuum model. *Computer Methods in Applied Mechanics and Engineering*, 191:21–28, 2001.

[14] T. S. Majmudar and R. P. Behringer. Contact force measurements and stress-induced anisotropy in granular materials. *Nature*, 435(7045):1079–1082, 2005.

[15] T. Matsushima. Effect of irregular grain shape on quasi-static shear behavior of granular assembly. In *Powders and Grains 05: Proc. of the Fifth International Conference on the Micromechanics of Granular Media*, volume 2, pages 1319–1323, 2005.

[16] T. Matsushima, J. Katagiri, K. Uesugi, A. Tsuchiyama, and T. Nakano. 3D shape characterization and image-based dem simulation of the lunar soil simulant FJS-1. *Journal of Aerospace Engineering*, 22:15–23, 2009.

[17] K. Mehlhorn and D. Michail. Implementing minimum cycle basis algorithms. *ACM Journal of Experimental Algorithmics*, 11(2.5):1–14, 2006.

[18] M. M. Mehrabadi and S. Nemat-Nasser. Stress, dilatency and fabric in granular materials. *Mechanics of Materials*, 2(2):155–161, 1983.

[19] R. Milo, S. Shen-Orr, S. Itzkovitz, N. Kashtan, D. Chklovskii, and U. Alon. Network motifs: simple building blocks of complex networks. *Science*, 298(5594):824–827, 2002.

[20] A. Munjiza. *The Combined Finite-Discrete Element Method*. John Wiley and Sons, 2004.

[21] M. E. J. Newman. The structure and function of complex networks. *SIAM Review*, 45(2):167–256, 2003.

[22] T. T. Ng. Fabric study of granular materials after compaction. *Journal of Engineering Mechanics*, 125(12):1390–1394, 1999.

[23] M. Oda and K. Iwashita, editors. *Mechanics of Granular Materials: An Introduction*. A. A. Balkema, Rotterdam, 1999.

[24] M. Oda and H. Kazama. Microstructure of shear bands and its relation to the mechanisms of dilatancy and failure of dense granular soils. *Geotechnique*, 48(4):465–481, 1998.

[25] Jukka-Pekka Onnela, Jari Saramäki, János Kertész, and Kimmo Kaski. Intensity and coherence of motifs in weighted complex networks. *Physical Review E*, 71:065103(R), 2005.

[26] A. D. Orlando and H. H. Shen. Effect of rolling friction on binary collisions of spheres. *Physics of Fluids*, 22:033304, 2010. doi:10.1063/1.3349728.

[27] J. F. Peters, M. A. Hopkins, R. Kala, and R. E. Wahl. A poly-ellipsoid particle for non-spherical discrete element method. *Engineering Computations*, 26(6):645–657, 2009.

[28] A. L. Rechenmacher. Grain-scale processes governing shear band initiation and evolution in sands. *Journal of Mechanics and Physics of Solids*, 54:22–45, 2006.

[29] L. Rothenburg and N. P. Kruyt. Critical state and evolution of coordinated number in simulated granular materials. *International Journal of Solids and Structures*, 41(21):5763–5774, 2004.

[30] A. Schofield and P. Wroth. *Critical State Soil Mechanics*. McGraw-Hill, New York, 1968.

[31] S. H. Strogatz. Exploring complex networks. *Nature*, 410:268–276, 2001.

[32] C. Thornton. Numerical simulations of deviatoric shear deformation of granular media. *Geotechnique*, 50:43–53, 2000.

[33] A. Tordesillas, Q. Lin, J. Zhang, R. P. Behringer, and J. Y. Shi. Structural stability of self-organized cluster conformations in dense granular materials. *Journal of Mechanics and Physics of Solids*, 2010. in review.

[34] A. Tordesillas and M. Muthuswamy. On the modelling of confined buckling of force chains. *Journal of the Mechanics and Physics of Solids*, 57:706–727, 2009.

[35] A. Tordesillas, P. OSullivan, D. M. Walker, and Paramitha. Evolution of functional connectivity in contact and force chain networks: feature vectors, k-cores and minimal cycles. *CRAS, Proceedings of the French Academy of Sciences (special issue invitation)*, 2010. in review.

[36] A. Tordesillas, J. Shi, and T. Tshaikiwsky. Stress-dilatancy and force chain evolution. *International Journal for Numerical and Analytical Methods in Geomechanics*, 2010. doi:10.1002/nag.910.

[37] A. Tordesillas, D. M. Walker, and Q. Lin. Force cycles and force chains. *Physical Review E*, 81:011302, 2010.

[38] A. Tordesillas and S. D. C. Walsh. Incorporating rolling resistance and contact anisotropy in micromechanical models of granular media. *Powder Technology*, 124(1–2):106–111, 2002.

[39] A. Tordesillas, J. Zhang, and R. Behringer. Buckling force chains in dense granular assemblies: physical and numerical experiments. *Geomechanics and Geoengineering*, 4:3–16, 2009.

[40] L. Uthus, M. A. Hopkins, and I. Horvli. Discrete element modeling of the resilient behavior of unbound granular aggregates. *International Journal of Pavement Engineering*, 9(6):387–395, 2008.

[41] M. van Hecke. Jamming of soft particles: geometry, mechanics, scaling and isostaticity. *Journal of Physics: Condensed Matter*, 22(3):033101, 2010.

[42] D. M. Walker and A. Tordesillas. Topological evolution in dense granular materials: a complex networks perspective. *International Journal of Solids and Structures*, 47:624–639, 2010.

[43] D. J. Watts and S. H. Strogatz. Collective dynamics of 'small-world' networks. *Nature*, 393:440–442, 1998.

[44] J. Zhang, T. S. Majmudar, A. Tordesillas, and R. P. Behringer. Statistical properties of a 2d granular materials subjected to cyclic shear. *Granular Matter*, 12:159–172, 2010.

Received Sep 2010; revised Nov 2010.

http://monotone.uwaterloo.ca/∼journal/